Chinese Journal of Natural Medicines

Design and synthesis of novel saponin–triazole derivatives in the regulation of adipogenesis

Yongsheng Fang, Zhiyun Zhu, Chun Xie, Dazhen Xia, Huimin Zhao, Zihui Wang, Qian Lu, Caimei Zhang, Wenyong Xiong, Xiaodong Yang

Citation: Yongsheng Fang, Zhiyun Zhu, Chun Xie, Dazhen Xia, Huimin Zhao, Zihui Wang, Qian Lu, Caimei Zhang, Wenyong Xiong, Xiaodong Yang, Design and synthesis of novel saponin–triazole derivatives in the regulation of adipogenesis, Chinese Journal of Natural Medicines, 2025, 23(8), 920–931. doi: 10.1016/S1875–5364(25)60830–2.

View online: https://doi.org/10.1016/S1875–5364(25)60830–2

Chinese Journal of Natural Medicines 23 (2025) 920-931

Contents lists available at ScienceDirect

Chinese Journal of Natural Medicines

journal homepage: www.cjnmcpu.com/

Original article

Design and synthesis of novel saponin-triazole derivatives in the regulation of adipogenesis

Yongsheng Fang[Δ], Zhiyun Zhu[Δ], Chun Xie, Dazhen Xia, Huimin Zhao, Zihui Wang, Qian Lu, Caimei Zhang, Wenyong Xiong[*], Xiaodong Yang[*]

Key Laboratory of Medicinal Chemistry for Natural Resource, Ministry of Education; Yunnan Key Laboratory of Research and Development for Natural Products, School of Pharmacy; Yunnan University, Kunming 650500, China

ARTICLE INFO

Article history:
Received 13 October 2024
Revised 27 December 2024
Accepted 2 February 2025
Available online 20 August 2025

Keywords:
Panax notoginseng
Saponin-triazole derivatives
Adipocyte differentiation and maturation
Lipid metabolism
Structure-activity relationships

ABSTRACT

Saponins associated with *Panax notoginseng* (*P. notoginseng*) demonstrate significant therapeutic efficacy across multiple diseases. However, certain high-yield saponins face limited clinical applications due to their reduced pharmacological efficacy. This study synthesized and evaluated 36 saponin-1,2,3-triazole derivatives of ginsenosides Rg1/Rb1 and notoginsenoside R1 for anti-adipogenesis activity *in vitro*. The research revealed that the ginsenosides Rg1-1,2,3-triazole derivative **a17** demonstrates superior adipogenesis inhibitory effects. Structure-activity relationships (SARs) analysis indicates that incorporating an amidyl-substituted 1,2,3-triazole into the saponin side chain *via* Click reaction enhances anti-adipogenesis activity. Additionally, several other derivatives exhibit general adipogenesis inhibition. Compound **a17** demonstrated enhanced potency compared to the parent ginsenoside Rg1. Mechanistic investigations revealed that **a17** exhibits dose-dependent inhibition of adipogenesis *in vitro*, accompanied by decreased expression of preadipocytes. Peroxisome proliferator-activated receptor γ (PPARγ), fatty acid synthase (FAS), and fatty acid binding protein 4 (FABP4) adipogenesis regulators. These findings establish the ginsenoside Rg1-1,2,3-triazole derivative **a17** as a promising adipocyte differentiation inhibitor and potential therapeutic agent for obesity and associated metabolic disorders. This research provides a foundation for developing effective therapeutic approaches for various metabolic syndromes.

1. Introduction

Obesity represents a significant global health challenge [1]. This condition serves as a primary contributor to numerous metabolic disorders, including type 2 diabetes mellitus (T2DM), non-alcoholic fatty liver disease (NAFLD), hypertension, cardiovascular diseases (CVDs), and cancer [2-7]. The World Health Organization (WHO) projects that the global population of overweight or obese adults will exceed 3 billion by 2030 [8, 9]. Current commercial anti-obesity medications have demonstrated limited efficacy and raised substantial safety concerns [10]. Consequently, the development of cost-effective, highly efficient anti-obesity medications with minimal adverse effects has become increasingly urgent.

Natural products serve as essential resources for human health maintenance, accounting for 63.1% of FDA-approved small molecule drugs between 1981 and 2019 [11, 12]. Research in natural products encompasses both direct application and the development of drug lead compounds [13]. Studies focusing on lead compound derivation have examined the relationship between structural characteristics and therapeutic activity. *Panax notoginseng* (*P. notoginseng*), an Araliaceae family member indigenous to Yunnan, China, represents a significant medicinal plant [14]. This species contains bioactive ginsenoside components that demonstrate efficacy in promoting blood circulation, resolving stasis, reducing swelling, and alleviating pain [15-18]. Scientists have isolated more than 80 triterpenoid saponins from *P. notoginsen*, with notoginsenoside R1 and ginsenosides Rg1, Re, Rb1, and Rd constituting the primary saponins in the plant root [19]. *P. notoginseng* saponins demonstrate significant pharmacological effects on adipogenesis inhibition and exhibit regulatory effects on obesity and lipid metabolism [20, 21]. These saponins inhibit adipogenesis by downregulating fatty acid synthase (FAS), sterol regulatory element-binding protein-1c (SREBP-1c), and stearoyl-CoA desaturase 1 (SCD1) through the adenosine 5'-monophosphate-activated protein kinase (AMPK) signaling pathway, thereby reducing white adipose tissue (WAT) weight and decreasing diabetic mice body weight [22]. Additionally, *P. notoginseng* saponins inhibit lipase protein expression in NAFLD and reduce WAT lipolysis, thus decreasing hepatic lipid accumulation [23]. Research on individual notoginsenoside monomers reveals that ginsenoside Rg1 increases uncoupling protein 1 (UCP1) expression and mitochondrial biogenesis in subcutaneous white adipose cells in 3T3-L1 and C57BL/6 mice, promoting adipocyte browning and exerting anti-obesity effects through AMPK pathway activation [24]. Similarly, ginsenoside Rb1 induces browning of 3T3-L1 cells and peri-

* Corresponding author.
E-mail addresses: xwy@ynu.edu.cn (W. Xiong); xdyang@ynu.edu.cn (X. Yang)
Δ These authors contributed equally to this work.

https://doi.org/10.1016/S1875-5364(25)60830-2

renal WAT (PWAT) *via* AMPK, demonstrating anti-obesity effects [25]. Furthermore, ginsenoside Rb1 enhances abnormal hepatic glucose metabolism in T2DM patients through STAT3-dependent mechanisms, suggesting potential therapeutic applications [26]. Current pharmacological research on *P. notoginseng* saponins and notoginsenoside monomers has primarily addressed CVDs, central nervous system disorders, and anti-cancer activities. Rare ginsenosides such as Rh2 and Rg5, present in minimal quantities in *P. notoginseng* saponins, demonstrate high bioactivity. Conversely, the primary components, including ginsenosides Rg1, Rb1, and notoginsenoside R1, exhibit relatively lower pharmacological activity [27-30] (Fig. 1). This study aims to enhance these saponins' practical value through structural modification.

Over the past three decades, molecular hybridization techniques have significantly contributed to targeted drug discovery across various diseases [31, 32]. Bioorthogonal coupling reactions have recently emerged as a powerful tool in drug development, providing advantages in lead compound screening, small molecule design strategies, and expanding the range of designed compounds [33-37]. Current research emphasizes the synthesis of multi-functional compounds containing 1,2,3-triazole structures through Click chemistry applications [38-47]. The triazole unit serves as a particularly valuable scaffold in medicinal chemistry, especially in addressing obesity and diabetes treatment [48-50] (Fig. 1). Building upon our previous research on natural product-like hybrids [51-58], this study examines the synthesis of 1,2,3-triazole derivatives of *P. notoginseng* saponin. The research evaluates their inhibitory activity in adipocyte differentiation and investigates structure-activity relationships (SARs). This represents the first reported synthesis and biological activity assessment of saponin-1,2,3-triazole derivatives. The study establishes cocktail-induced 3T3-L1 adipocytes to evaluate regulatory effects and presents a preliminary anti-obesity mechanism using Western blotting and molecular docking (Fig. 1).

2. Results and discussion

2.1. Chemistry

As illustrated in Scheme 1, the high polarity of saponins, due to their sugar moieties, significantly affects separation and reaction post-treatment. Therefore, protecting the saponin hydroxyl groups is essential. Starting with commercially available ginsenosides Rg1 (**a1**), ginsenosides Rb1 (**b1**), and notoginsenoside R1 (**c1**), the hydroxyl groups underwent complete protection through acetylation with acetic anhydride, using 4-dimethylaminopyridine (DMAP) as a catalyst, producing acetylated products **a2**, **b2** and **c2**. The double bonds in compounds **a2**, **b2**, and **c2** were then cleaved by ozone at −78 °C, followed by sodium borohydride reduction to generate alcohols **a3**, **b3**, and **c3**. Using triethylamine as a base, compounds **a3**, **b3**, and **c3** underwent esterification with methanesulfonyl chloride (MsCl) to form methanesulfonate esters. Under reflux conditions with sodium iodide in acetone solvent, iodine substitution products **a4**, **b4**, and **c4** were produced. Compounds **a5**, **b5**, and **c5** were obtained through nucleophilic substitution reactions with sodium azide (NaN_3) at 60 °C. Finally, through Click reactions using anhydrous copper (II) acetate and sodium ascorbate as catalysts, the target derivative products ginsenoside Rg1-triazole **a6**–**a17**, ginsenoside Rb1-triazole **b6**–**b17**, and notoginsenoside R1-triazole **c6**–**c17** were synthesized using various terminal alkynes, achieving 57%–85% yields. Table 1 presents the structures and yields of these new 1,2,3-triazole derivatives.

2.2. Anti-adipogenesis activities of ginsenosides Rg1, Rb1, and notoginsenoside R1 derivatives

The 3T3-L1 preadipocyte cell line serves as a well-established cellular model for studying fat metabolism, capable of differentiating into mature white adipocytes under specific conditions [59]. To evaluate the inhibitory effects on adipocyte differentiation, 36 synthesized 1,2,3-triazole derivatives of ginsenoside Rg1 (**a6**–**a17**), ginsenoside Rb1 (**b6**–**b17**), and notoginsenoside R1 (**c6**–**c17**) were tested on 3T3-L1 preadipocyte differentiation. The study employed LiCl as a positive control, while differentiation was induced using a combination of isobutylmethylxanthine (IBMX), dexamethasone (DEX), insulin (INS), and rosiglitazone (ROSI) [60, 61]. The preadipocyte differentiation process during the induction period is illustrated in Fig. 2A. After completing the differentiation process, lipid content in the 3T3-L1 cells was evaluated using Oil Red O staining for visualization and quantific-

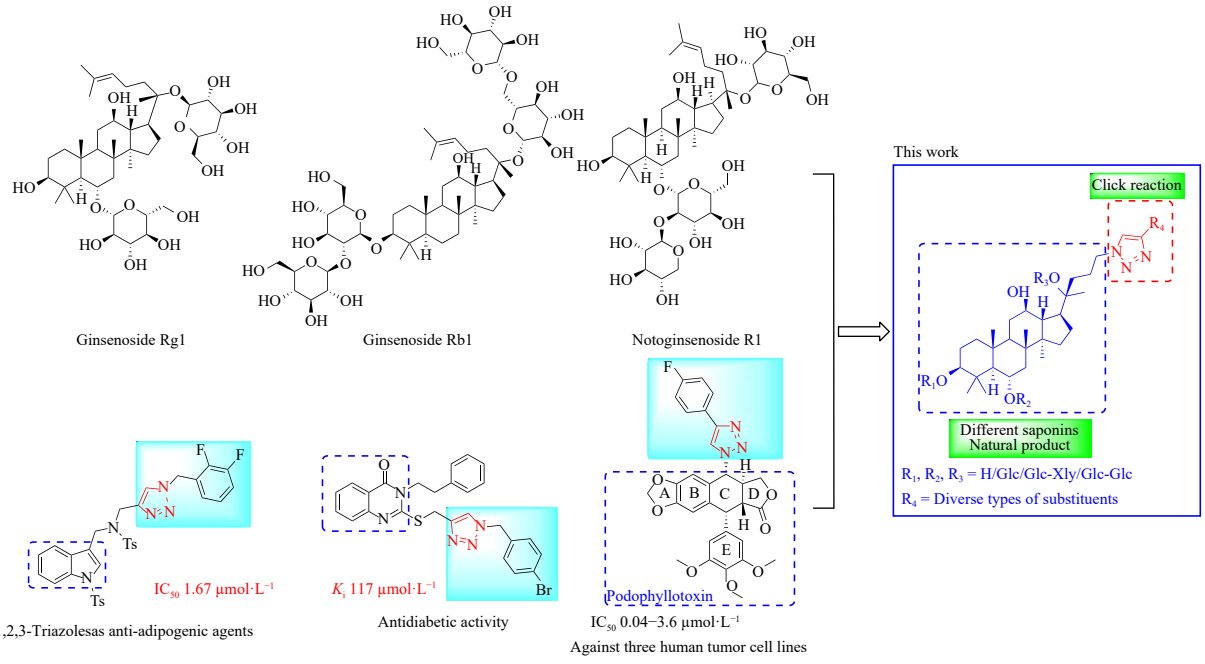

Fig. 1 Structures of ginsenosides Rg1, Rb1, and notoginsenoside R1, 1,2,3-triazole-containing hybrids as leads in medicinal chemistry and the design of saponin derivatives.

ation. The results indicated that ginsenoside Rg1-1,2,3-triazole derivative **a17** decreased lipid accumulation in adipocytes at 30 μmol·L^{-1}. Quantification of intracellular lipid content aligned with Oil Red O staining observations (Fig. 2B). Among all tested compounds, **a17** demonstrated the highest inhibitory activity (Fig. 2C). Based on these findings regarding activity and stability, compound **a17** was selected for further investigation of its effects on preadipocyte viability and molecular mechanisms in adipogenesis regulation.

2.3. SARs

The structural characteristics of ginsenosides Rg1, Rb1, and notoginsenoside R1 derivatives demonstrating significant inhibitory activity represent crucial factors in controlling cell differentiation and maturation of 3T3-L1 preadipocytes. Through the introduction of the 1,2,3-triazole pharmacophore *via* Click reaction, ginsenoside Rg1 derivatives **a6**–**a17**, ginsenoside Rb1 derivatives **b6**–**b17**, and notoginsenoside R1 derivatives **c6**–**c17** exhib-

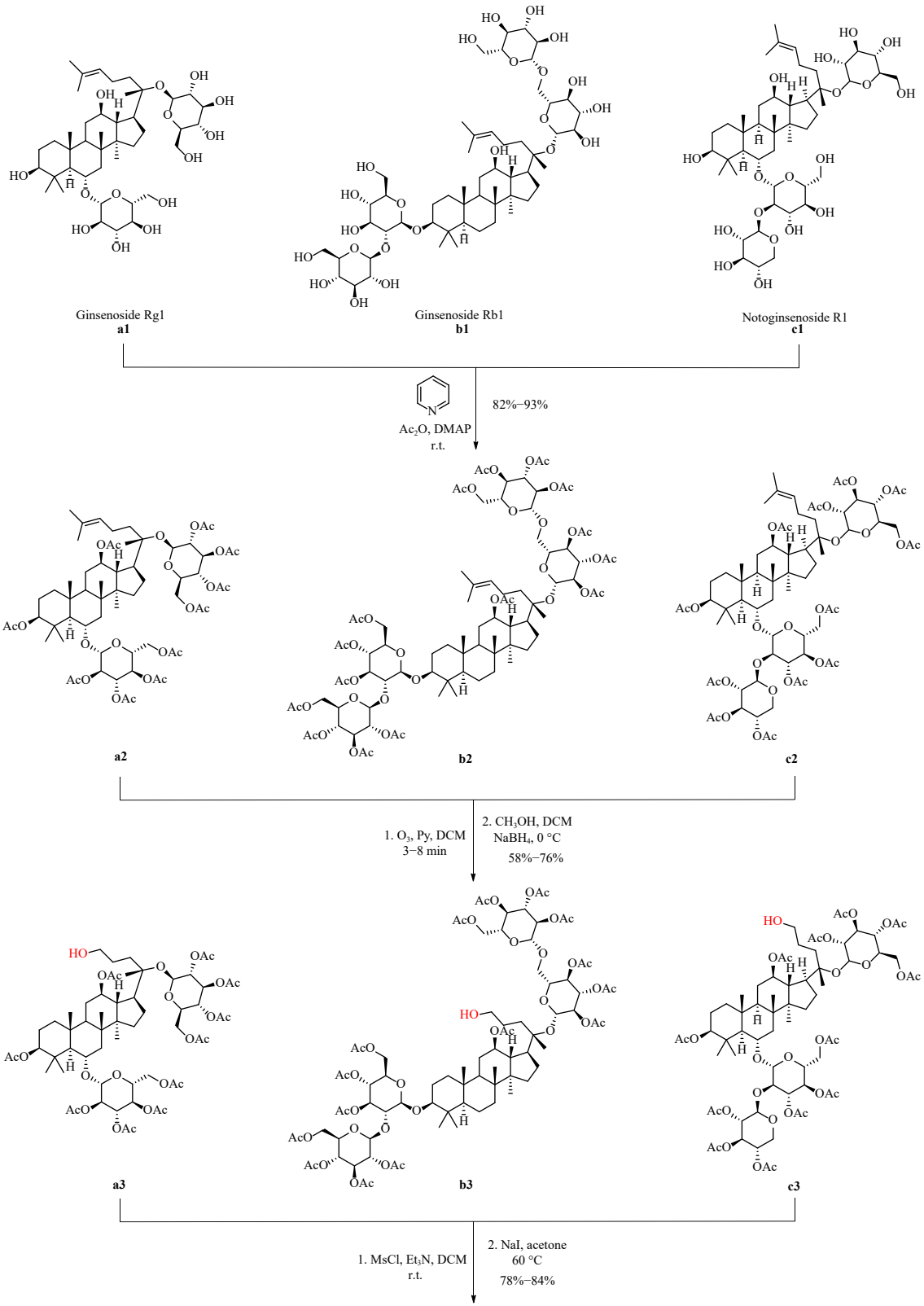

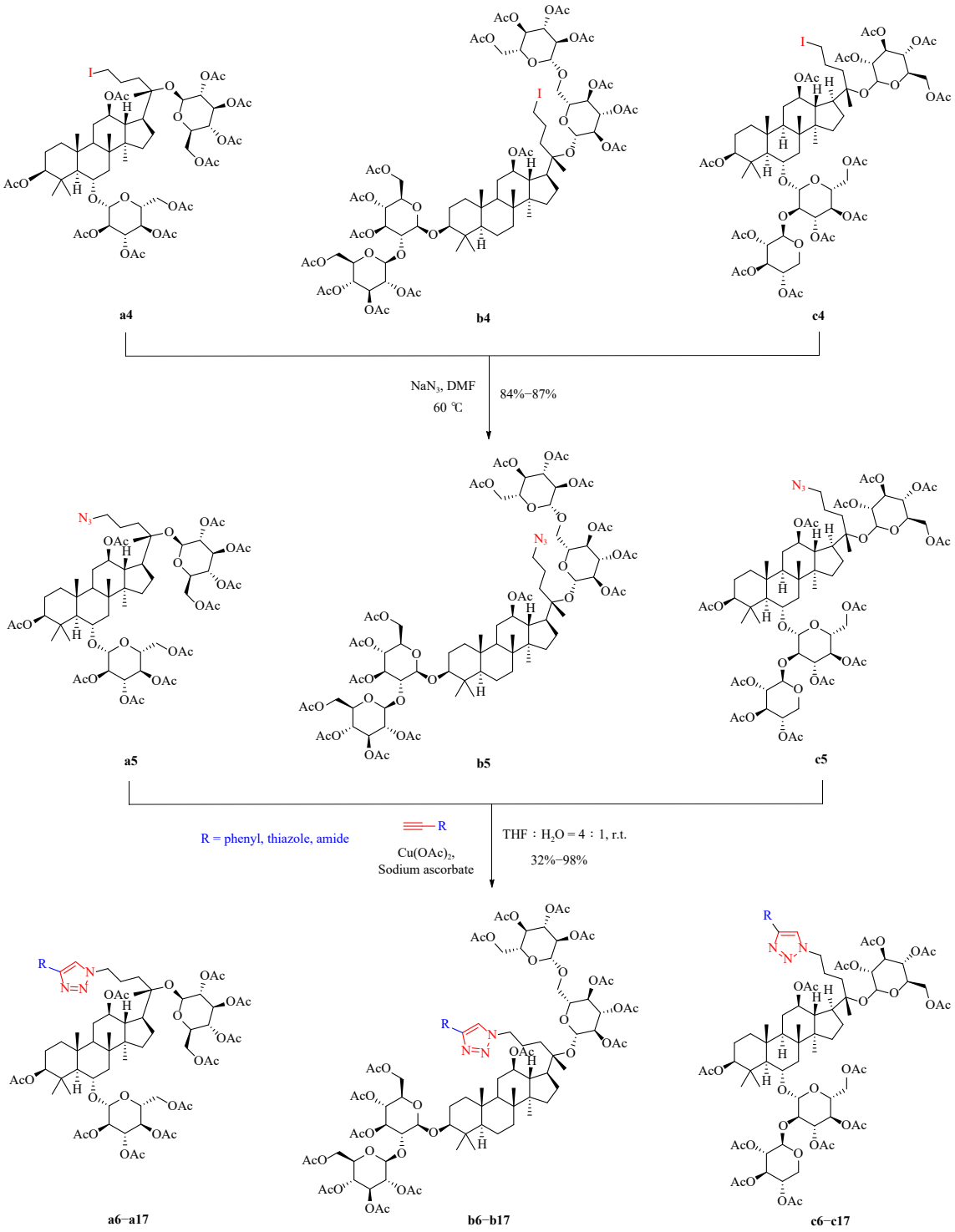

Scheme 1 Synthesis of 1,2,3-triazole derivatives of ginsenosides Rg1 (**a6–a17**), Rb1 (**b6–b17**) and notoginsenoside R1 (**c6–c17**).

ited enhanced inhibitory activity compared to their parent compounds. The inhibition rates ranged from 16.6% to 45.7%. Among these compounds, ginsenoside Rg1 derivative **a17** demonstrated the highest efficacy in inhibiting adipocyte differentiation and maturation. Subsequent investigations focused on examining the effects of the optimal compound **a17** on preadipocyte viability and elucidating the molecular mechanisms underlying its dose-dependent inhibition of differentiation, maturation, and adipogenesis regulation in white adipocytes.

Regarding the structural characteristics of saponin, ginsenoside Rb1 derivatives **b6–b17** contain more glycosidic bonds than ginsenoside Rg1 derivatives **a6–a17** and notoginsenoside R1 derivatives **c6–c17**, potentially resulting in increased molecular weight of the ginsenoside Rb1 derivatives and decreased cell membrane permeability and fat solubility. The inhibitory effect of the Rb1 derivatives **b6–b17** was marginally lower than that observed for ginsenoside Rg1 derivatives **a6–a17** and notoginsenoside R1 derivatives **c6–c17**.

Examining R group substituents on the 1,2,3-triazole ring, electron-withdrawing groups (R = NO_2, F, Cl and Br, **a8/b8/c8**, **a10/b10/c10**, **a11/b11/c11**, **a12/b12/c12**) demonstrated higher inhibitory activity, with inhibition rates of 26.0%–41.9%. For electron-donating groups (R = NH_2, OMe and CH_3, **a7/b7/c7**, **a9/b9/c9** and **a13/b13/c13**), inhibitory activity was lower, ran-

Table 1 Structures and yields of 1,2,3-triazole derivatives of ginsenosides Rg1, Rb1, and notoginsenoside R1.

Entry	Compound No.	Saponins	R	Molecular formula	Yields/%
1	**a6**	Ginsenoside Rg1	Pyridine	$C_{66}H_{92}N_4O_{24}$	36
2	**a7**	Ginsenoside Rg1	Aniline	$C_{67}H_{94}N_4O_{24}$	72
3	**a8**	Ginsenoside Rg1	Fluorobenzene	$C_{67}H_{92}FN_3O_{24}$	81
4	**a9**	Ginsenoside Rg1	Methoxybenzine	$C_{68}H_{95}N_3O_{25}$	78
5	**a10**	Ginsenoside Rg1	Chlorobenzene	$C_{67}H_{92}ClN_3O_{24}$	80
6	**a11**	Ginsenoside Rg1	Bromobenzene	$C_{67}H_{92}BrN_3O_{24}$	74
7	**a12**	Ginsenoside Rg1	Nitrobenzene	$C_{67}H_{92}N_4O_{26}$	81
8	**a13**	Ginsenoside Rg1	Toluene	$C_{68}H_{95}N_3O_{24}$	62
9	**a14**	Ginsenoside Rg1	Benzene	$C_{67}H_{93}N_3O_{24}$	85
10	**a15**	Ginsenoside Rg1	Naphthalene	$C_{71}H_{95}N_3O_{24}$	86
11	**a16**	Ginsenoside Rg1	Thiophene	$C_{65}H_{91}N_3O_{24}S$	98
12	**a17**	Ginsenoside Rg1	Acetamide	$C_{62}H_{90}N_4O_{25}$	62
13	**b6**	Ginsenoside Rb1	Pyridine	$C_{88}H_{122}N_4O_{38}$	36
14	**b7**	Ginsenoside Rb1	Aniline	$C_{89}H_{124}N_4O_{38}$	32
15	**b8**	Ginsenoside Rb1	Fluorobenzene	$C_{89}H_{122}FN_3O_{38}$	74
16	**b9**	Ginsenoside Rb1	Methoxybenzine	$C_{90}H_{125}N_3O_{39}$	62
17	**b10**	Ginsenoside Rb1	Chlorobenzene	$C_{89}H_{122}ClN_3O_{38}$	88
18	**b11**	Ginsenoside Rb1	Bromobenzene	$C_{89}H_{122}BrN_3O_{38}$	76
19	**b12**	Ginsenoside Rb1	Nitrobenzene	$C_{89}H_{122}N_4O_{40}$	75
20	**b13**	Ginsenoside Rb1	Toluene	$C_{90}H_{125}N_3O_{38}$	89
21	**b14**	Ginsenoside Rb1	Benzene	$C_{89}H_{123}N_3O_{38}$	81
22	**b15**	Ginsenoside Rb1	Naphthalene	$C_{93}H_{125}N_3O_{38}$	85
23	**b16**	Ginsenoside Rb1	Thiophene	$C_{87}H_{121}N_3O_{38}S$	83
24	**b17**	Ginsenoside Rb1	Acetamide	$C_{84}H_{120}N_4O_{39}$	40
25	**c6**	Notoginsenoside R1	Pyridine	$C_{75}H_{104}N_4O_{30}$	57
26	**c7**	Notoginsenoside R1	Aniline	$C_{76}H_{106}N_4O_{30}$	71
27	**c8**	Notoginsenoside R1	Fluorobenzene	$C_{76}H_{104}FN_3O_{30}$	72
28	**c9**	Notoginsenoside R1	Methoxybenzine	$C_{77}H_{107}N_3O_{31}$	76
29	**c10**	Notoginsenoside R1	Chlorobenzene	$C_{76}H_{104}ClN_3O_{30}$	85
30	**c11**	Notoginsenoside R1	Bromobenzene	$C_{76}H_{104}BrN_3O_{30}$	79
31	**c12**	Notoginsenoside R1	Nitrobenzene	$C_{76}H_{104}N_4O_{32}$	73
32	**c13**	Notoginsenoside R1	Toluene	$C_{77}H_{107}N_3O_{30}$	68
33	**c14**	Notoginsenoside R1	Benzene	$C_{76}H_{105}N_3O_{30}$	79
34	**c15**	Notoginsenoside R1	Naphthalene	$C_{80}H_{107}N_3O_{30}$	84
35	**c16**	Notoginsenoside R1	Thiophene	$C_{74}H_{103}N_3O_{30}S$	69
36	**c17**	Notoginsenoside R1	Acetamide	$C_{71}H_{102}N_4O_{31}$	65

ging from 16.6%–29.1%. With pyridine as the substituent group, the inhibitory activity of **a6/b6/c6** decreased due to electron-withdrawing effects, showing inhibition rates of 17.1%–32.2%. The naphthalene ring substituent introduced significant steric hindrance, with **a15/b15/c15** showing inhibition rates of 23.6%–40.8%. The heterocyclic thiophene ring substituent in **a16/b16/c16** produced moderate inhibitory activity (23.8%–34.5%). Notably, amide substitution enhanced conjugation effects, with amide derivatives **a17/b17/c17** exhibiting optimal inhibitory activity (31.5%–45.7%).

The findings indicate that incorporating amide-substituted 1,2,3-triazole derivatives in a ginsenoside Rg1 Click reaction significantly inhibited adipocyte differentiation and maturation. The preliminary SARs for the derivatives are summarized in Scheme 2.

*2.4. Dose dependence in **a17** inhibited adipogenesis*

The 3T3-L1 cell line serves as a standard *in vitro* cellular model for examining adipocyte development and function. This

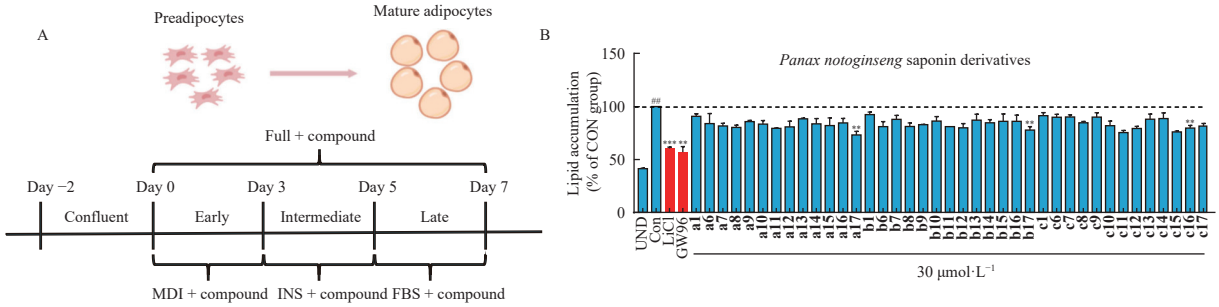

C

Entry	Compound No.	Inhibition rate/%	Entry	Compound No.	Inhibition rate/%	Entry	Compound No.	Inhibition rate/%
1	**a1**	15.6	14	**b1**	12.9	27	**c1**	14.6
2	**a6**	27.1	15	**b6**	32.2	28	**c6**	17.1
3	**a7**	31.0	16	**b7**	20.6	29	**c7**	16.6
4	**a8**	33.5	17	**b8**	32.0	30	**c8**	26.0
5	**a9**	24.1	18	**b9**	29.1	31	**c9**	16.9
6	**a10**	28.3	19	**b10**	23.3	32	**c10**	30.6
7	**a11**	35.1	20	**b11**	32.2	33	**c11**	41.9
8	**a12**	32.9	21	**b12**	34.2	34	**c12**	35.3
9	**a13**	19.6	22	**b13**	21.7	35	**c13**	20.3
10	**a14**	27.9	23	**b14**	25.9	36	**c14**	19.2
11	**a15**	30.3	24	**b15**	23.6	37	**c15**	40.8
12	**a16**	26.4	25	**b16**	23.8	38	**c16**	34.5
13	**a17**	45.7	26	**b17**	37.8	39	**c17**	31.5
40	LiCl	67.1	41	GW9662	57.1			

Inhibitionrate (%) = [(Con − UND) − (As − UND)]/(Con − UND) × 100; As: Experimental group absorbance.

Data represent the mean values of three independent determinations.

Fig. 2 Activity screening of saponin-triazole derivatives on anti-adipogenesis and the predicted binding mode of the protein-ligand complex. (A) Schematic of the protocol for induction of adipocyte differentiation and administration of ginsenosides Rg1, Rb1, and notoginsenoside R1 derivatives. (B) Normalized quantification of lipids in adipocytes by measuring Oil Red O intensity of the cells. Ginsenosides Rg1 (30 μmol·L^{-1}), Rb1 (30 μmol·L^{-1}), notoginsenoside R1 (30 μmol·L^{-1}), GW9662 (50 μmol·L^{-1}) and LiCl (20 mmol·L^{-1}) were used as positive controls. (C) Inhibition rate of ginsenosides Rg1, Rb1, and notoginsenoside R1 derivatives (**a6–a17**, **b6–b17**, and **c6–c17**) *in vitro*. The data were presented as mean ± SEM (n = 3). $^{\#\#}P < 0.01$ *vs* the UND group; $^{*}P < 0.05$ and $^{**}P < 0.01$ *vs* the CON group.

cell line provides an optimal model system for investigating the regulation of differentiation-related genes during adipocyte differentiation [62]. During differentiation, preadipocytes activate multiple adipogenic genes through transcription factor regulation, initiating complex physiological and biochemical processes that culminate in mature adipocyte formation. Excessive differentiation leads to adipocyte proliferation, contributing to adipose tissue expansion associated with obesity development and progression. Therefore, inhibiting preadipocyte differentiation represents a potential strategy for obesity prevention. In this investigation, **a17** was administered (at concentrations of 3.75, 7.5, 15, 30, 60, and 90 μmol·L^{-1}) to the medium during adipocyte differentiation, producing varying effects on the differentiation process. Microscopic examination revealed decreased intracellular lipid droplets with increasing **a17** concentration. Additionally, higher **a17** concentrations corresponded to an increased proportion of cells displaying a non-lipid droplet phenotype (Fig. 3A). The quantification of liquid droplet dissolution appears in Fig. 3B. At the conclusion of induction differentiation on day seven, adipocytes treated with sequential **a17** concentrations showed decreased lipid content by −0.1%, 10%, 22.1%, 53.0%, 65.4%, and 75.3% compared to the CON. Based on Fig. 3B results, Prism software analysis determined the half-maximal inhibitory concentration (IC_{50}) value of **a17** on adipocyte differentiation as 29.78 μmol·L^{-1} (Fig. 3C).

The MTS assay was utilized to evaluate **a17**'s effect on cell viability by exposing preadipocytes to concentrations of 15, 30, 60, 120, and 160 μmol·L^{-1} **a17** for 24 h. Results shown in Fig. 3D indicate that even the highest **a17** concentration (160 μmol·L^{-1}) did not produce significant cytotoxicity, indicating that the inhibition of white adipocyte differentiation is not attributable to cytotoxic effects. These results demonstrate that **a17** inhibited adipocyte differentiation in a dose-dependent manner within a safe concentration range.

*2.5. Regulation of adipogenesis by **a17** in the middle stage of differentiation*

As 3T3-L1 preadipocytes undergo differentiation, the expression of adipocyte-specific genes increases significantly, establishing the molecular foundation for terminal maturation. Key transcriptional regulators such as peroxisome proliferator-activated receptor γ (PPARγ) and CCAAT/enhancer-binding proteins (C/EBPs) play central roles in determining adipocyte fate [63–65]. Additionally, fatty acid synthase (FAS) and fatty acid-binding protein 4 (FABP4) are pivotal in lipid anabolism, promoting lipid synthesis and storage [66]. Based on prior findings indicating that **a17** modulates adipogenesis in a concentration-dependent manner, we further investigated its effect on the expression of these adipogenic markers at the protein level. GW9662, a selective PPARγ antagonist known to inhibit adipocyte differentiation, was used as a positive control. In the untreated differentiation control group (CON), the expression levels of PPARγ, FAS, and FABP4 were markedly increased. Treatment with **a17** at concentrations of 15, 30, 60, and 90 μmol·L^{-1} led to a dose-dependent downregulation of these proteins. In contrast, the expression of

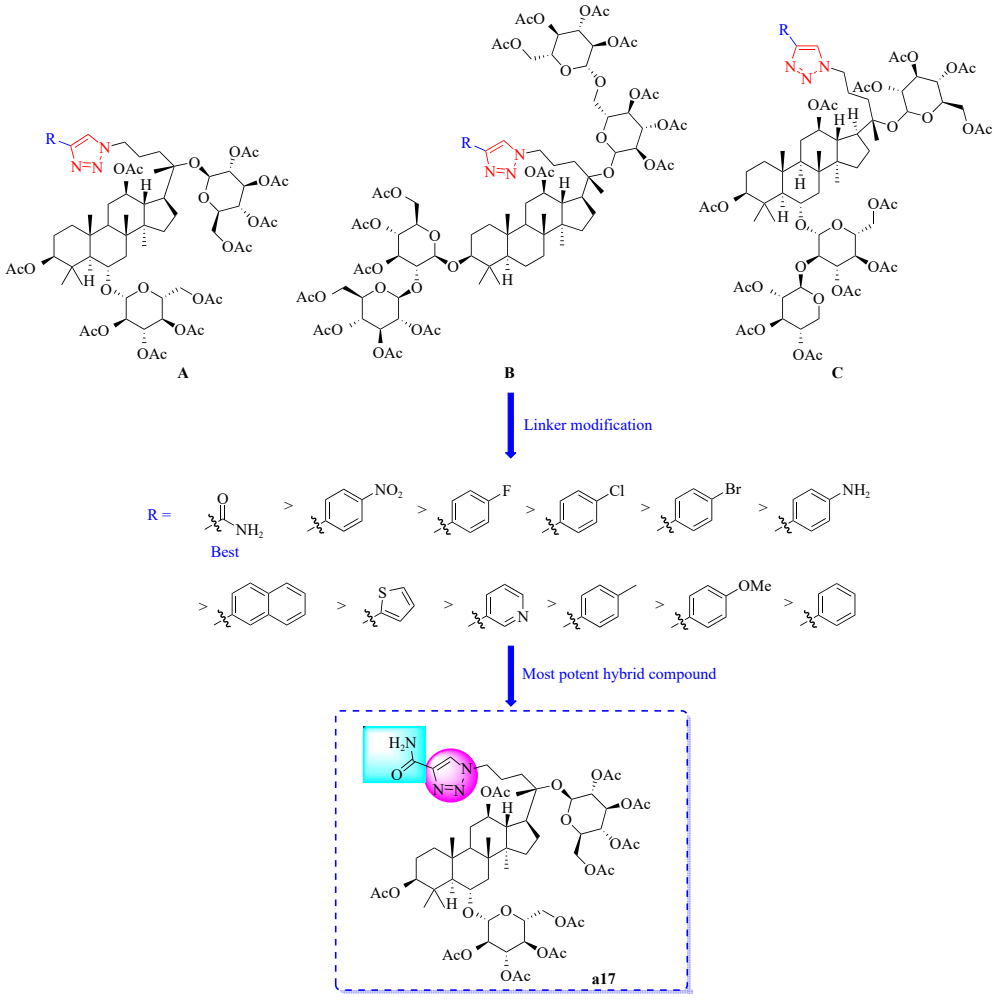

Scheme 2 Structure-activity relationship of ginsenosides Rg1, Rb1, and notoginsenoside R1 derivatives.

C/EBPβ, an early adipogenic transcription factor, remained unaffected by **a17** (Fig. 4A). These findings are further supported by the data presented in Figs. 4B–4E, reinforcing the notion that **a17** selectively attenuates late-stage adipogenic signaling without interfering with early-stage differentiation regulators.

2.6. Molecular docking

To elucidate the mechanism underlying the high activity of compound **a17**, molecular docking analysis was conducted using Autodock vina. Fig. 5A illustrates the binding sites of compound **a17** in the protein, where the glucose side chain of the **a17** molecule is embedded within the structure. As depicted in Fig. 5B, compound **a17** established 4 hydrogen bonds with the residues. The amide nitrogen atom of **a17** formed 2 hydrogen bonds with residues SER225. Furthermore, the oxygen atom on the glucose side chain of the saponin parent nucleus and the acetyl protection group formed 2 strong hydrogen bonds with residue SER342. Two additional residues, PRO227 and GLY284, contributed to the docking interaction. The residues SER225 and SER342 were identified as crucial amino acids for inhibitor binding.

Molecular docking analyses were also performed for compounds **b17** and **c17** using the same computational parameters. Both compounds exhibited measurable binding affinity toward the target protein, but their binding modes differed significantly. In Fig. 5E, the glucose side chain of compound **c17** was able to insert into the binding pocket of the protein, similar to the conformation observed for compound **a17**. However, in Fig. 5C, shows that for compound **b17**, the glucose side chain projected outward, while the triazole moiety instead inserted into the pocket. Compound **b17** formed a single hydrogen bond with residue SER342 (Fig. 5D), whereas no hydrogen bonding was observed in the docking pose of compound **c17** (Fig. 5F). This lack of specific interactions may partially explain the lower biological activity of compound **c17** compared to **b17**.

To investigate the influence of different substituents on biological activity, molecular docking operations were conducted on all compounds of the A series. Ten models were generated, and the optimal model was selected for comparative analysis.

Compound **a17** achieved the second-highest docking score. Notably, while the electron-withdrawing nitro group exhibited the highest score, its biological activity was not optimal. The electron-withdrawing groups (R = F, Cl, Br) demonstrated comparable scores. The electron-donating groups (R = NH_2, OCH_3, CH_3) showed considerable score variation. Compound **a9** (R = OCH_3) achieved the third highest score despite its limited biological activity. Heterocyclic structures, including pyridine and naphthalene, showed moderate scores, consistent with their biological activity data. Compound **a16**, containing a thiophene substituent, maintained moderate biological activity despite its lowest docking score. Overall, the molecular docking scores demonstrated a correlation with the biological activity test results.

3. Conclusion

A series of novel *P. notoginseng* saponin-1,2,3-triazole derivatives have been synthesized, demonstrating significant inhibition of adipocyte differentiation. The synthesis included various

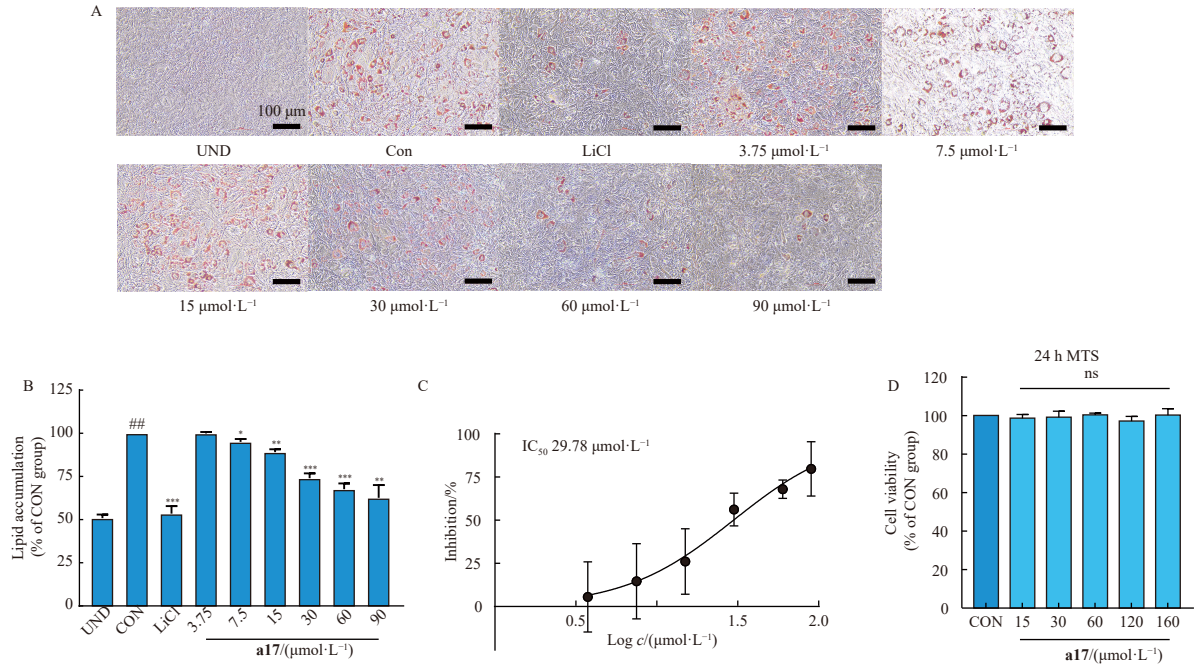

Fig. 3 **a17** suppressed the differentiation of adipocytes and related protein expressions. (A) Representative Oil Red O-stained images of 3T3-L1 adipocytes treated with increasing concentrations of **a17** (3.75–90 μmol·L^{-1}). Scale bar = 100 μm. (B) Quantification of intracellular lipid accumulation based on Oil Red O absorbance. (C) IC $_{50}$ value of **a17** for adipogenesis inhibition, calculated using GraphPad Prism. (D) Cell viability of 3T3-L1 preadipocytes treated with **a17** (15–160 μmol·L^{-1}) for 24 h, assessed by MTS assay. Data are presented as mean ± SEM (n = 3). $^{\#\#}P < 0.01$ *vs* the UND group; $^{*}P < 0.05$, $^{**}P < 0.01$, and $^{***}P < 0.001$ *vs* the CON group; ns: no significance compared to the CON group.

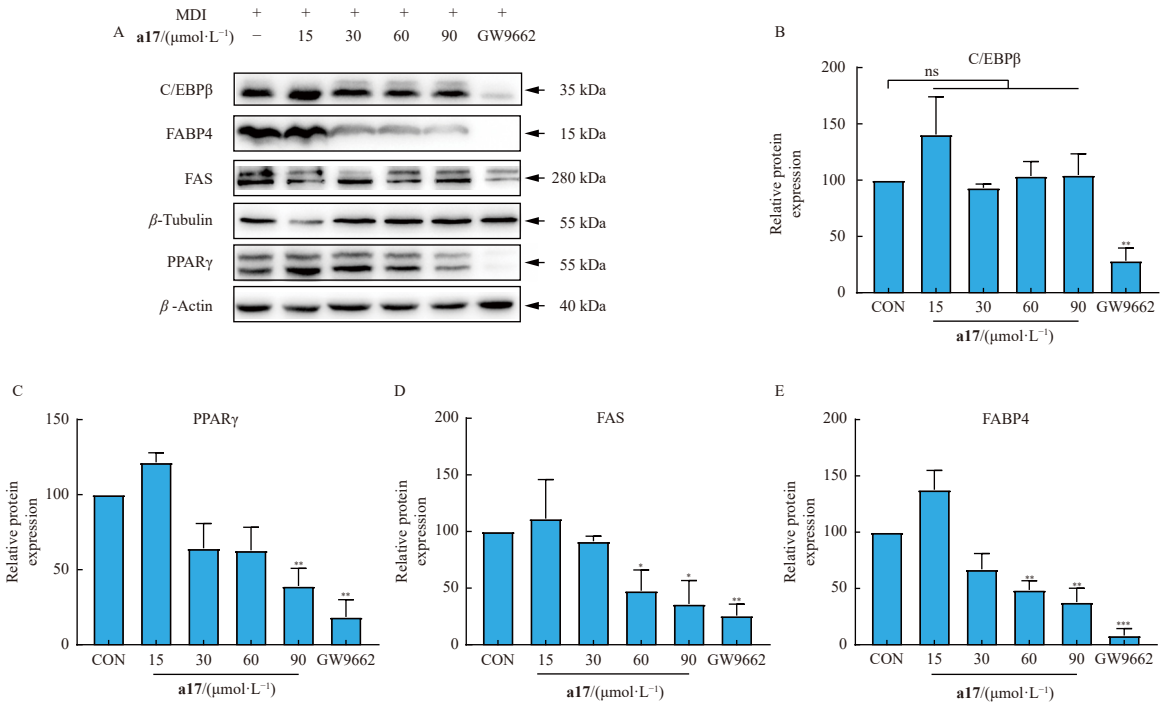

Fig. 4 (A) Images of Western blotting bands showing the expression levels of C/EBPβ, PPARγ, FAS, and FABP4 in 3T3-L1 adipocytes treated with varying concentrations of. (B–E) Quantified and normalized protein expression levels of C/EBPβ, PPARγ, FAS, and FABP4, respectively. The data were presented as mean ± SEM (n = 3). $^{*}P < 0.05$, $^{**}P < 0.01$ and $^{***}P < 0.001$ *vs* the CON group; ns: no significance compared to the CON group.

1,2,3-triazole derivatives of ginsenoside Rg1, ginsenoside Rb1, and notoginsenoside R1, which exhibited substantial inhibitory activity against adipocyte differentiation and maturation. Analysis revealed that incorporating electron-withdrawing substituent groups on the 1,2,3-triazole derivatives *via* Click reaction enhanced their effectiveness in inhibiting adipocyte differentiation and maturation. The ginsenoside Rg1 derivative **a17** containing an amide substitution group demonstrated superior inhibition (45.7%). Additionally, **a17** showed dose-dependent inhibition of adipocyte differentiation within safe concentration parameters. The effects of **a17** included downregulation of adipogenic transcription factors crucial for promoting adipogenesis and maintaining adipocyte differentiation, specifically targeting PPARγ, FAS, and FABP4. These results indicate that the Rg1-1,2,3-triazole derivative **a17** represents a promising lead compound for adipogenesis inhibition. Subsequent research will focus on

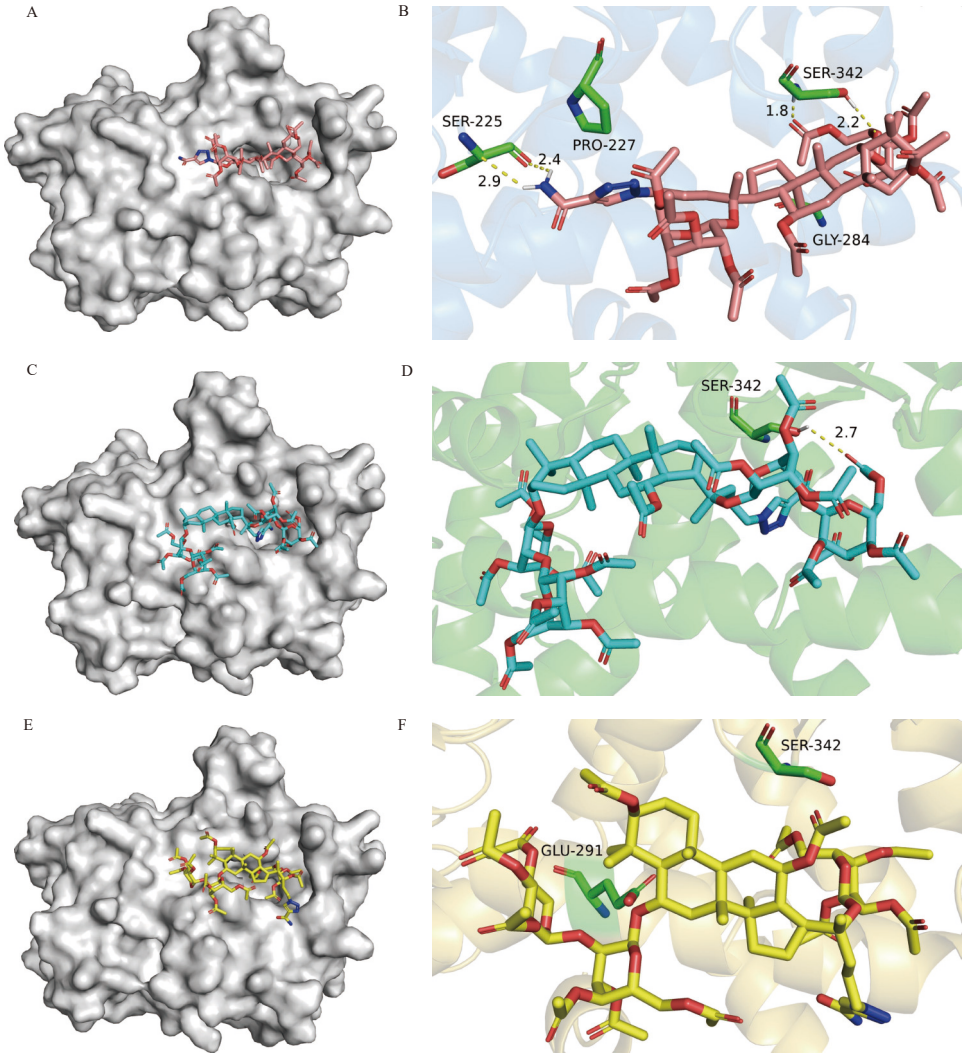

Fig. 5 Predicted binding modes of PPARγ with compounds **a17**, **b17**, and **c17**. (A, C, E) Overall docking poses of PPARγ in complex with compound **a17** (orange sticks), **b17** (cyan sticks), and **c17** (yellow sticks), respectively. (B, D, F) Enlarged views of the ligand-receptor binding interface. Hydrogen bonds are shown as yellow dashed lines.

comprehensive structural modifications and mechanistic studies, advancing the development of more effective and economical anti-obesity medications.

4. Experimental

4.1. Materials

Melting points were determined and uncorrected using a Haineng melting-point apparatus (MP430, Jinan, China). Proton nuclear magnetic resonance (^{1}H NMR) spectra were obtained on Bruker Avance 400 and Bruker Avance 600 spectrometers (Bruker, MA, USA) at 400 MHz and 600 MHz. Carbon-13 nuclear magnetic resonance (^{13}C NMR) was recorded on Bruker Avance 400 spectrometer at 100 MHz and Bruker Avance 600 spectrometer at 150 MHz (Bruker, MA, USA). Chemical shifts are expressed as δ values relative to tetramethylsilane (TMS) for all recorded NMR spectra. High-resolution mass spectra were acquired using an Agilent LC-MSO/TOR mass spectrometer (Agilent Technologies, CA, USA). Silica gel (200–300 mesh) for column chromatography and silica GF_{254} for TLC were obtained from Qingdao Marine Chemical Company (Qingdao, China). All air- or moisture-sensitive reactions were performed under an argon atmosphere. Starting materials and reagents were sourced commercially from TCI, Adamas, Aladdin, and Bidepharm and used without further purification, unless specified otherwise.

4.2. Synthesis of compounds *a2/b2/c2*

To a solution of ginsenoside Rg1 (**a1**, 4.0 g, 5.0 mmol) in pyridine (30 mL) was added acetic anhydride (Ac_2O, 9.45 mL, 100.0 mmol) and 4-dimethylaminopyridine (DMAP, 0.12 g, 1.0 mmol). The reaction mixture was stirred at room temperature for 12 h, then quenched with 4.0 mol·L^{-1} aqueous HCl (100 mL). The mixture was extracted with ethyl acetate (EtOAc, 3 × 150 mL), and the combined organic layers were washed successively with saturated aqueous $NaHCO_3$ (150 mL) and brine (150 mL), dried over Na_2SO_4, and concentrated under reduced pressure. The crude product was purified by silica gel column chromatography using a gradient of DCM∶EtOAc, 5∶1 to 2∶1, yielding **a2** as a white powder (93% yield).

Ginsenoside Rb1 (**b1**, 5.5 g, 5.0 mmol) was treated under identical conditions using pyridine (30 mL), acetic anhydride (14.18 mL, 150.0 mmol), and DMAP (0.12 g, 1.0 mmol). After 12 h of stirring at room temperature and standard aqueous work-up, the product was purified by silica gel chromatography using a DCM∶EtOAc gradient from 3∶1 to 1∶1, affording compound **b2** as a white powder (82% yield).

Notoginsenoside R1 (**c1**, 4.66 g, 5.0 mmol) was dissolved in pyridine (30 mL) and reacted with acetic anhydride (11.34 mL, 120.0 mmol) and DMAP (0.12 g, 1.0 mmol) under the same condi-

tions. Following quenching, extraction, and purification by column chromatography (DCM∶EtOAc, 3∶1 to 1∶1), compound **c2** was obtained as a white powder in 93% yield. Complete physical and spectroscopic characterization data for compounds **a2**, **b2**, and **c2** are provided in the Supporting information.

*4.3. Synthesis of compounds **a3–a5/b3–b5/c3–c5***

To a solution of compound **a2** (4.88 g, 4.0 mmol)/**b2** (6.96 g, 4.0 mmol)/**c2** (5.75 g, 4.0 mmol) in DCM (30.0 mL), a few drops of pyridine were added. The resulting mixture was stirred and cooled at −78 °C for several minutes before introducing ozone for 3–8 min (monitored by TLC). Upon reaction completion, the solution was transferred to an ice water bath. MeOH (5 mL) was added to the round bottom flask, followed by a slow addition of $NaBH_4$ (454 mg, 12 mmol). After removing the ice bath, the solution was stirred for 2 h at room temperature before quenching with NH_4Cl (1 mL, sat. aq.) and concentrating *in vacuo*. Column chromatography purification of the residue (silica gel, DCM∶EA, 1∶1) afforded **a3/b3/c3** in 58%–76% yield (two steps) as white powder (Physical and spectral data of **a3/b3/c3** are included in the Supporting information).

To a solution of compound **a3** (2.63 g, 2.2 mmol)/**b3** (3.77 g, 2.2 mmol)/**c3** (3.10 g, 2.2 mmol) in DCM (30.0 mL), MsCl (340 μL, 4.4 mmol) and Et_3N (612 μL, 4.4 mmol) were added. The mixture was stirred at room temperature for 12 h before quenching with H_2O (30 mL). After separating the layers, the organic layer underwent extraction with CH_2Cl_2 (3 × 30 mL), drying over (Na_2SO_4) and concentration *in vacuo*. The residue was dissolved in acetone (30 mL), treated with NaI (989 mg, 6.6 mmol) and stirred at 60 °C for 12 h before quenching with H_2O (30 mL) and diluting with EtOAc (30 mL). Following layer separation, the organic layer was extracted with EtOAc (3 × 30 mL), dried over (Na_2SO_4) and concentrated *in vacuo*. Column chromatography purification of the residue (silica gel, DCM∶EA, 3∶1) yielded **a4/b4/c4** in 78%–84% yield (two steps) as white or yellow powder (Physical and spectral data of **a4/b4/c4** are included in the Supporting information).

To a solution of compound **a4** (2.22 g, 1.7 mmol)/**b4** (3.10 g, 1.7 mmol)/**c4** (2.59 g, 1.7 mmol) in DMF (30.0 mL), NaN_3 (221 mg, 3.4 mmol) was added. The mixture was stirred at 80 °C for 12 h before being quenched with H_2O (30 mL) and diluted with EtOAc (30 mL). The layers were separated, and the organic layer was extracted with EtOAc (3 × 30 mL), dried (Na_2SO_4) and concentrated *in vacuo*. The residue underwent purification by column chromatography (silica gel, DCM∶EA, 3∶1) to yield **a5/b5/c5** at 84%–87% as white powder (Physical and spectral data of **a5/b5/c5** are included in the Supporting information).

*4.4. Synthesis of compounds **a6–a17/b6–b17/c6–c17***

To a solution of compound **a5/b5/c5** (0.05 mmol) in THF (4.0 mL), alkyne (0.1 mmol), $Cu(OAc)_2$ (0.075 mmol), sodium ascorbate (0.1 mmol) and water (1 mL) were sequentially added. The mixture was stirred at room temperature for 12 h and concentrated *in vacuo*. The residue underwent purification by column chromatography (silica gel, DCM∶EA, 5∶1 to 1∶1) to yield **a6–a17/b6–b17/c6–c17** at 32%–98% as white or brown powder (Physical and spectral data of **a6–a17/b6–b17/c6–c17** are included in the Supporting information).

4.5. Cell, differentiation, and treatment

Mouse 3T3-L1 preadipocytes were obtained from the American Type Culture Collection (ATCC, USA) and cultured in a 5% CO_2 humidified incubator at 37 °C (Phcbi, Tokyo, Japan). Cells were maintained in high-glucose Dulbecco's Modified Eagle Medium (DMEM) supplemented with 10% newborn bovine serum and 1% penicillin-streptomycin (P/S). Upon reaching complete confluency (designated as day 0), differentiation was induced by treating the cells with an adipogenic induction cocktail consisting of 1 μmol·L^{-1} DEX, 0.5 mmol·L^{-1} IBMX, 1 μmol·L^{-1} ROSI, and 1 μg·mL^{-1} INS in DMEM containing 10% FBS. This induction phase was maintained for 3 d. On day 3, the induction medium was replaced with DMEM containing 10% FBS and 1 μg·mL^{-1} insulin, and the cells were cultured for additional 2 d. Subsequently, the medium was changed to DMEM supplemented with 10% FBS alone, and the cells were incubated for another 2 d to complete the differentiation process.

4.6. Oil Red O staining

Following adipocyte differentiation induction, the cells underwent the following procedures: washing three times with phosphate-buffered saline (PBS) and fixation in 10% formalin at room temperature for 1 h. The cells were then rinsed twice with distilled water, once with 60% isopropanol, and maintained for 3 min. Subsequently, staining occurred with Oil Red O working solution for 15 min, followed by four rinses with distilled water. The cells were photographed using a Nikon inverted microscope and a Nikon digital camera system (Nikon, Tokyo, Japan). For quantitative analysis, Oil Red O staining was performed, and the stain was eluted with 100% isopropanol. Absorbance measurements were conducted at 492 nm.

4.7. Cell viability assay

Cell viability was assessed using the MTS method. Initially, 3T3-L1 preadipocytes were seeded in 96-well plates at a density of 1 × 10^5 cells·mL^{-1} and incubated for 2 d. Distilled water was added to the peripheral wells as a control, while the remaining wells received 150 μL of culture medium. Various concentrations of **a17** were administered and incubated for 24 h at 37 °C. Following incubation, the cell culture medium was removed, and MTS solution was added to each well. The plates were incubated for an additional 2 h at 37 °C. The absorbance was then measured at 492 nm using a microplate reader (Thermo, MA, USA) to determine cell viability.

4.8. Whole-cell extracts and Western blotting analysis

Prior to harvesting, both untreated and **a17** treated cells were washed twice with pre-chilled PBS. The cells were then lysed in RIPA lysis buffer containing 2 mmol·L^{-1} PMSF (Med Chem Express, China). Cell lysates were obtained by scrapping the cells for 15 min on ice, followed by centrifugation at 10 000 *g* for 10 min at 4 °C to collect the supernatant. Total protein concentration was determined using a BCA protein assay kit. The protein samples were denatured by heating at 100 °C for 10 min. Equal amounts of protein were separated using 8%–13% sodium dodecyl sulfate-polyacrylamide gel electrophoresis and transferred onto polyvinylidene fluoride (PVDF) membranes. The membranes were blocked with PBS-T (1 × PBS and 0.1% Tween-20, pH 7.6) containing 5% non-fat dry milk for 1 h on a shaker. The membranes were then incubated overnight at 4 °C with primary antibodies. After washing, the secondary antibody was added and incubated for 2 h at room temperature. Bands were visualized using enhanced chemiluminescent reagents and an imaging system (5200 Multi, Tanon, China), and photographs were captured. Quantitative analysis of band grayscale values was conducted using MetaMoph software.

4.9. Statistical analysis

All data were expressed as mean ± standard error of the

mean (SEM). To compare the differences between the two groups, an unpaired *t*-test was performed using GraphPrism 9.5 software. $P < 0.05$ was considered statistically significant.

Funding

This work was supported by the Central Government Guides Local Science and Technology Development Fund (Nos. 202207AA110007, 202207AB110002), Yunnan Science and Technology Department (No. 202402AA310009), the Program for Xingdian Talents (Yun-Ling Scholars) and IRTSTYN.

Availability of supporting information

Supporting information for this study can be obtained by contacting the corresponding authors *via* E-mail.

Declaration of competing interest

These authors have no conflict of interest to declare.

References

1 De Lorenzo A, Gratteri S, Gualtieri P, et al. Why primary obesity is a disease. *J Transl Med*. 2019;17(1):169. https://doi.org/10.1186/s12967-019-1919-y.
2 Jin X, Qiu T, Li L, et al. Pathophysiology of obesity and its associated diseases. *Acta Pharm Sin B*. 2023;13(6):2403-2424. https://doi.org/10.1016/j.apsb.2023.01.012.
3 Geng J, Ni Q, Sun W, et al. The links between gut microbiota and obesity and obesity related diseases. *Biomed Pharmacother*. 2022;147:112678. https://doi.org/10.1016/j.biopha.2022.112678.
4 Su HG, Wang Q, Zhou L, et al. Highly oxygenated lanostane triterpenoids from *Ganoderma applanatum* as a class of agents for inhibiting lipid accumulation in adipocytes. *Bioorg Chem*. 2020;104:104263. https://doi.org/10.1016/j.bioorg.2020.104263.
5 Su HG, Wang Q, Zhou L, et al. Functional triterpenoids from medicinal fungi *Ganoderma applanatum*: a continuous search for antiadipogenic agents. *Bioorg Chem*. 2021;112:104977. https://doi.org/10.1016/j.bioorg.2021.104977.
6 Kelly T, Yang W, Chen CS, et al. Global burden of obesity in 2005 and projections to 2030. *Int J Obesity*. 2008;32(9):1431-1437. https://doi.org/10.1038/ijo.2008.102.
7 Valenzuela PL, Carrera-Bastos P, Castillo-Garcia A, et al. Obesity and the risk of cardiometabolic diseases. *Nat Rev Cardiol*. 2023;20(7):475-494. https://doi.org/10.1038/s41569-023-00847-5.
8 de Klerk MT, Smeets PAM, la Fleur SE. Inhibitory control as a potential treatment target for obesity. *Nutr Neurosci*. 2023;26(5):429-444. https://doi.org/10.1080/1028415X.2022.2053406.
9 Wang Y, Wang L, Qu W. New national data show alarming increase in obesity and noncommunicable chronic diseases in China. *Eur J Clin Nutr*. 2017;71(1):149-150. https://doi.org/10.1038/ejcn.2016.171.
10 Corkey BE, Apovian CM. "En attendant godot": waiting for the answer to obesity and longevity. *Obesity*. 2022;30(11):2105-2106. https://doi.org/10.1002/oby.23462.
11 Luo Z, Yin F, Wang X, et al. Progress in approved drugs from natural product resources. *Chin J Nat Med*. 2024;22(3):195-211. https://doi.org/10.1016/S1875-5364(24)60582-0.
12 Newman DJ, Cragg GM. Natural products as sources of new drugs over the nearly four decades from 01/1981 to 09/2019. *J Nat Prod*. 2020;83(3):770-803. https://doi.org/10.1021/acs.jnatprod.9b01285.
13 Shen B. A new golden age of natural products drug discovery. *Cell*. 2015;163(6):1297-1300. https://doi.org/10.1016/j.cell.2015.11.031.
14 Yang WZ, Bo T, Ji S, et al. Rapid chemical profiling of saponins in the flower buds of *Panax notoginseng* by integrating MCI gel column chromatography and liquid chromatography/mass spectrometry analysis. *Food Chem*. 2013;139:762-769. https://doi.org/10.1016/j.foodchem.2013.01.051.
15 Yousof AM, Jannat S, Mizanur RM. Ginsenoside derivatives inhibit advanced glycation end-product formation and glucose–fructose mediated protein glycation *in vitro via* a specific structure–activity relationship. *Bioorg Chem*. 2021;111:104844. https://doi.org/10.1016/j.bioorg.2021.104844.
16 Guo YP, Shao L, Chen MY, et al. *In vivo* metabolic profiles of *Panax notoginseng* saponins mediated by gut microbiota in rats. *J Agr Food Chem*. 2020;68(25):6835-6844. https://doi.org/10.1021/acs.jafc.0c01857.
17 Qiu S, Yang WZ, Yao CL, et al. Malonylginsenosides with potential antidiabetic activities from the flower buds of *Panax ginseng*. *J Nat Prod*. 2017;80(4):899-908. https://doi.org/10.1021/acs.jnatprod.6b00789.
18 Wang T, Guo R, Zhou G, et al. Traditional uses, botany, phytochemistry, pharmacology and toxicology of *Panax notoginseng* (Burk.) F. H. Chen: a review. *J Ethnopharmacol*. 2016;188:234-258. https://doi.org/10.1016/j.jep.2016.05.005.
19 Gu CZ, Lv JJ, Zhang XX, et al. Triterpenoids with promoting effects on the differentiation of PC12 cells from the steamed roots of *Panax notoginseng*. *J Nat Prod*. 2015;78(8):1829-1840. https://doi.org/10.1021/acs.jnatprod.5b00027.
20 Xu Y, Wang N, Tan HY, et al. Gut-liver axis modulation of *Panax notoginseng* saponins in nonalcoholic fatty liver disease. *Hepatol Int*. 2021;15(2):350-365. https://doi.org/10.1007/s12072-021-10138-1.
21 Yang JW, Kim S. Ginsenoside Rc promotes anti-adipogenic activity on 3T3-L1 adipocytes by down-regulating C/EBPα and PPARγ. *Molecules*. 2015;20(1):1293-1303. https://doi.org/10.3390/molecules20011293.
22 Wang Q, Mu RF, Liu X, et al. Steaming changes the composition of saponins of *Panax notoginseng* (Burk.) F. H. Chen that function in treatment of hyperlipidemia and obesity. *J Agr Food Chem*. 2020;68(17):4865-4875. https://doi.org/10.1021/acs.jafc.0c00746.
23 Ding RB, Tian K, Cao YW, et al. Protective effect of *Panax notoginseng* saponins on acute ethanol-induced liver injury is associated with ameliorating hepatic lipid accumulation and reducing ethanol-mediated oxidative stress. *J Agr Food Chem*. 2015;63(9):2413-2422. https://doi.org/10.1021/jf502990n.
24 Lee K, Seo YJ, Song JH, et al. Ginsenoside Rg1 promotes browning by inducing UCP1 expression and mitochondrial activity in 3T3-L1 and subcutaneous white adipocytes. *J Ginseng Res*. 2019;43(4):589-599. https://doi.org/10.1016/j.jgr.2018.07.005.
25 Park SJ, Park M, Sharma A, et al. Black ginseng and ginsenoside Rb1 promote browning by inducing UCP1 expression in 3T3-L1 and primary white adipocytes. *Nutrients*. 2019;11:2747. https://doi.org/10.3390/nu11112747.
26 Wang W, Zhan W, Liang M, et al. Ginsenoside Rb1 ameliorates the abnormal hepatic glucose metabolism by activating STAT3 in T2DM mice. *J Funct Foods*. 2023;104:105534. https://doi.org/10.1016/j.jff.2023.105534.
27 Peng H, Chen L, Deng Y, et al. Ginsenoside Rh2 mitigates myocardial damage in acute myocardial infarction by regulating pyroptosis of cardiomyocytes. *Clin Exp Hypertens*. 2023;45(1):1-7. https://doi.org/10.1080/10641963.2023.2229536.
28 Li X, Chu S, Lin M, et al. Anticancer property of ginsenoside Rh2 from ginseng. *Eur J Med Chem*. 2020;203:112627. https://doi.org/10.1016/j.ejmech.2020.112627.
29 Zhu Y, Yang H, Deng J, et al. Ginsenoside Rg5 improves insulin resistance and mitochondrial biogenesis of liver *via* regulation of the Sirt1/PGC-1α signaling pathway in db/db mice. *J Agr Food Chem*. 2021;69(30):8428-8439. https://doi.org/10.1021/acs.jafc.1c02476.
30 Xia W, Zhu Z, Xiang S, et al. Ginsenoside Rg5 promotes wound healing in diabetes by reducing the negative regulation of SLC7A11 on the efferocytosis of dendritic cells. *J Ginseng Res*. 2023;47(6):784-794. https://doi.org/10.1016/j.jgr.2023.06.006.
31 Zhang H, Tian Y, Kang D, et al. Discovery of uracil-bearing DAPYs derivatives as novel HIV-1 NNRTIs *via* crystallographic overlay-based molecular hybridization. *Eur J Med Chem*. 2017;130:209-222. https://doi.org/10.1016/j.ejmech.2017.02.047.
32 Berube G. An overview of molecular hybrids in drug discovery. *Expert Opin Drug Dis*. 2016;11(3):281-305. https://doi.org/10.1517/17460441.2016.1135125.
33 Lemmon MA, Schlessinger J. Cell signaling by receptor tyrosine kinases. *Cell*. 2010;141(7):1117-1134. https://doi.org/10.1016/j.cell.2010.06.011.
34 Thirumurugan P, Matosiuk D, Jozwiak K. Click chemistry for drug development and diverse chemical-biology applications. *Chem Rev*. 2013;113(7):4905-4979. https://doi.org/10.1021/cr200409f.
35 Jiang X, Hao X, Jing L, et al. Recent applications of click chemistry in drug discovery. *Expert Opin Drug Dis*. 2019;14(8):779-789. https://doi.org/10.1080/17460441.2019.1614910.
36 Brighty GJ, Botham RC, Li S, et al. Using sulfuramidimidoyl fluorides that undergo sulfur(VI) fluoride exchange for inverse drug discovery. *Nat Chem*. 2020;12(10):906-913. https://doi.org/10.1038/s41557-020-0530-4.
37 Sletten EM, Bertozzi CR. Bioorthogonal chemistry: fishing for selectivity in a sea of functionality. *Angew Chem Int Edit*. 2009;48(38):6974-9698. https://doi.org/10.1002/anie.200900942.
38 Kondengadan SM, Bansal S, Yang C, et al. Click chemistry and drug delivery: a bird's-eye view. *Acta Pharm Sin B*. 2023;13(5):1990-2016. https://doi.org/10.1016/j.apsb.2022.10.015.
39 Bozorov K, Zhao J, Aisa HA. 1,2,3-Triazole-containing hybrids as leads in medicinal chemistry: a recent overview. *Bioorgan Med Chem*. 2019;27(16):3511-3531. https://doi.org/10.1016/j.bmc.2019.07.005.
40 Abdul Rahman SM, Bhatti JS, Thareja S, et al. Current development of 1,2,3-triazole derived potential antimalarial scaffolds: structure activity relationship (SAR) and bioactive compounds. *Eur J Med Chem*. 2023;259:115699. https://doi.org/10.1016/j.ejmech.2023.115699.
41 Daher SS, Lee M, Jin X, et al. Alternative approaches utilizing click chemistry to develop next-generation analogs of solithromycin. *Eur J Med Chem*. 2022;233:114213. https://doi.org/10.1016/j.ejmech.2022.114213.
42 Nguyen BCQ, Takahashi H, Uto Y, et al. 1,2,3-Triazolyl ester of ketorolac: a "click chemistry"-based highly potent PAK1-blocking cancer-killer. *Eur J Med Chem*. 2017;126:270-276. https://doi.org/10.1016/j.ejmech.2016.11.038.
43 Zhao S, Liu J, Lv Z, et al. Recent updates on 1,2,3-triazole-containing hybrids with *in vivo* therapeutic potential against cancers: a mini-review. *Eur J Med Chem*. 2023;251:115254. https://doi.org/10.1016/j.ejmech.2023.115254.
44 Zhang L, Zhang X, Yao Z, et al. Discovery of fluorogenic diarylsydnone-alkene photoligation: conversion of ortho-dual-twisted diarylsydnones into planar pyrazolines. *J Am Chem Soc*. 2018;140(24):7390-7394. https://doi.org/10.1021/jacs.8b02493.
45 Wang FC, Peng B, Ren TT, et al. A 1,2,3-triazole derivative of quinazoline exhibits antitumor activity by tethering RNF168 to SQSTM1/P62. *J Med Chem*. 2022;65(22):15028-15047. https://doi.org/10.1021/acs.jmedchem.2c00432.
46 Bhardwaj A, Kaur J, Wuest M, et al. *In situ* click chemistry generation of cyclooxygenase-2 inhibitors. *Nat Commun*. 2017;8(1):1-14. https://doi.org/10.1038/s41467-016-0009-6.

47 Bonandi E, Christodoulou MS, Fumagalli G, et al. The 1,2,3-triazole ring as a bioisostere in medicinal chemistry. *Drug Discov Today*. 2017;22(10):1572-1581. https://doi.org/10.1016/j.drudis.2017.05.014.

48 Avula SK, Khan A, Rehman NU, et al. Synthesis of 1*H*-1,2,3-triazole derivatives as new *α*-glucosidase inhibitors and their molecular docking studies. *Bioorg Chem*. 2018;81:98-106. https://doi.org/10.1016/j.bioorg.2018.08.008.

49 Saeedi M, Mohammadi-Khanaposhtani M, Pourrabia P, et al. Design and synthesis of novel quinazolinone-1,2,3-triazole hybrids as new anti-diabetic agents: *in vitro α*-glucosidase inhibition, kinetic, and docking study. *Bioorg Chem*. 2019;83:161-169. https://doi.org/10.1016/j.bioorg.2018.10.023.

50 Rajan S, Puri S, Kumar D, et al. Novel indole and triazole based hybrid molecules exhibit potent anti-adipogenic and antidyslipidemic activity by activating Wnt3a/*β*-catenin pathway. *Eur J Med Chem*. 2018;143:1345-1360. https://doi.org/10.1016/j.ejmech.2017.10.034.

51 Deng G, Zhou B, Wang J, et al. Synthesis and antitumor activity of novel steroidal imidazolium salt derivatives. *Eur J Med Chem*. 2019;168:232-252. https://doi.org/10.1016/j.ejmech.2019.02.025.

52 Liu LX, Wang XQ, Yan JM, et al. Synthesis and antitumor activities of novel dibenzo[b, d]furan-imidazole hybrid compounds. *Eur J Med Chem*. 2013;66:423-437. https://doi.org/10.1016/j.ejmech.2013.06.011.

53 Wang XQ, Liu LX, Li Y, et al. Design, synthesis and biological evaluation of novel hybrid compounds of imidazole scaffold-based 2-benzylbenzofuran as potent anticancer agents. *Eur J Med Chem*. 2013;62:111-121. https://doi.org/10.1016/j.ejmech.2012.12.040.

54 Yin M, Fang Y, Sun X, et al. Synthesis and anticancer activity of podophyllotoxin derivatives with nitrogen-containing heterocycles. *Front Chem*. 2023;11:1191498. https://doi.org/10.3389/fchem.2023.1191498.

55 Huang M, Duan S, Ma X, et al. Synthesis and antitumor activity of aza-brazilan derivatives containing imidazolium salt pharmacophores. *Medchemcomm*. 2019;10(6):1027-1036. https://doi.org/10.1039/C9MD00112C.

56 Zhou B, Liu ZF, Deng GG, et al. Synthesis and antitumor activity of novel *N*-substituted tetrahydro-*β*-carboline-imidazolium salt derivatives. *Org Biomol Chem*. 2016;14(39):9423-9430. https://doi.org/10.1039/C6OB01495J.

57 Liu JM, Wang M, Zhou YJ, et al. Novel 3-substituted fluorine imidazolium/triazolium salt derivatives: synthesis and antitumor activity. *RSC Adv*. 2015;5(78):63936-63944. https://doi.org/10.1039/C5RA07947K.

58 Liu LX, Wang XQ, Zhou B, et al. Synthesis and antitumor activity of novel *N*-substituted carbazole imidazolium salt derivatives. *Sci Rep-UK*. 2015;5:13101. https://doi.org/10.1038/srep13101.

59 Cho HH, Jang SH, Won C, et al. Derhamnosylmaysin inhibits adipogenesis *via* inhibiting expression of PPARγ and C/EBPα in 3T3-L1 cells. *Molecules*. 2022;27(13):4232. https://doi.org/10.3390/molecules27134232.

60 Liu DW, Ye YS, Huang CG, et al. Sampsonione F suppresses adipogenesis *via* activating p53 pathway during the mitotic clonal expansion progression of adipocyte differentiation. *Eur J Pharmacol*. 2022;925:175002. https://doi.org/10.1016/j.ejphar.2022.175002.

61 Zhou J, Zhang J, Li J, et al. Ginsenoside F2 suppresses adipogenesis in 3T3-L1 cells and obesity in mice *via* the AMPK pathway. *J Agr Food Chem*. 2021;69(32):9299-9312. https://doi.org/10.1021/acs.jafc.1c03420.

62 Cowherd RM, Lyle RE, Jr McGehee RE. Molecular regulation of adipocyte differentiation. *Semin Cell Dev Biol*. 1999;10(1):3-10. https://doi.org/10.1006/scdb.1998.0276.

63 Farmer SR. Transcriptional control of adipocyte formation. *Cell Metab*. 2006;4(4):263-273. https://doi.org/10.1016/j.cmet.2006.07.001.

64 Zhao L, Gregoire F, Sook SH. Transient induction of ENC-1, a Kelch-related actin-binding protein, is required for adipocyte differentiation. *J Biol Chem*. 2000;275(22):16845-16850. https://doi.org/10.1074/jbc.275.22.16845.

65 Lefterova MI, Lazar MA. New developments in adipogenesis. *Trends Endocrin Met*. 2009;20(3):107-114. https://doi.org/10.1016/j.tem.2008.11.005.

66 Liu S, Wu D, Fan Z, et al. FABP4 in obesity-associated carcinogenesis: novel insights into mechanisms and therapeutic implications. *Front Mol Biosci*. 2022;9:1-14. https://doi.org/10.3389/fmolb.2022.973955.